Mechanistic Insights into the Structural Asymmetry of the LanFEG Transporter NisFEG in Lantibiotic Immunity

Pablo A. Cea[1], Julia Gottstein[2], Sander H.J. Smits[2,3,5], Holger Gohlke[1,4,5]*

[1]Institut for Pharmaceutical and Medicinal Chemistry, Heinrich Heine University Düsseldorf, Düsseldorf, Germany

[2]Institute of Biochemistry, Heinrich Heine University Düsseldorf, Düsseldorf, Germany

[3] Center for Structural Studies, Heinrich Heine University Düsseldorf, Düsseldorf, Germany

[4]Institute of Bio- and Geosciences (IBG-4: Bioinformatics), Forschungszentrum Jülich GmbH, Jülich, Germany

[5]Interfaculty Center for Membrane Research, Heinrich Heine University Düsseldorf, 40225 Düsseldorf, Germany

Keywords: Nisin, NisFEG, LanFEG, lantibiotic, molecular simulations

Running title head: Structural Asymmetry of LanFEG Transporters in Lantibiotic Immunity

* Corresponding author

Tel.: +49-211-81-13662

Email: gohlke@uni-duesseldorf.de

Abstract

Nisin is one of the best studied antimicrobial peptides. Still, how nisin-producing strains can protect themselves against nisin's bactericidal effects is only partially understood. Located within the nisin biosynthesis operon, the heterotetrameric ABC transporter NisFEG transports nisin to the extracellular environment, granting autoimmunity to the producer strain. NisFEG belongs to the LanFEG family of ABC transporters, members of which are found in some lantibiotic-producing bacterial strains. However, their structure has not been elucidated. In this work, we constructed a full atom model of NisFEG in the ATP-bound conformation. The architecture of the complex reveals a narrow transmembrane interface with prominent lateral clefts, similar to those observed in other exporters of hydrophobic compounds. Through molecular dynamics (MD) simulations, we observed that one of the most conserved elements of the LanFEG family, the E-loop of the nucleotide binding domain, interacts preferentially with a small intracellular helix of the NisG transmembrane chain. Cosolvent MD simulations reveal the presence of a putative binding site within the lateral cleft of the transporter, next to the transmembrane chain NisE. Mutational analysis showed that large hydrophobic residues near this putative site are relevant to the transporter function, and more so than analogous residues in the opposite cleft. Our results suggest that nisin extrusion operates in an asymmetric manner, where contacts between the E-loop and NisG are the driving force for the conformational changes triggered by ATP hydrolysis, whereas the NisE subunit is the main mediator of interactions with the lantibiotic. This functional asymmetry could provide an explanation for why the LanFEG family has evolved two distinct transmembrane chains, where each one was selected to perform a single step in an optimal way, maximizing the immunity of lantibiotic-producing bacteria.

Introduction

Bacteria produce antimicrobial peptides (AMPs) that target closely related species for survival. These peptides are produced under stress conditions, including limited nutrient availability or nutrient starvation, and are produced by both Gram-(+) and Gram-(-) bacteria and usually possess a narrow spectrum antibacterial activity. Bacteriocins are a class of AMPs of particular interest since they can exert different modes of action in both genera.

Lanthipeptides are a class of bacteriocins that are produced by specific biosynthetic clusters mainly in Gram-positive bacteria, but their occurrence is not restricted to this group; they are also found in Gram-negative bacteria [1] and cyanobacteria [2, 3]. They are ribosomally synthesized as pre-peptides and undergo heavy post-translational modifications (PTMs) and are activated after secretion by a specific protease. The most distinctive PTMs occur on serine and threonine residues that are dehydrated, resulting in the non-standard α,β-unsaturated amino acids 2,3-didehydroaline (Dha) and 2,3-didehydobutyrine (Dhb) [4, 5], followed by a Michael-type condensation of these amino acids with cysteine residues, yielding a thioether crosslink, so-called lanthionine rings (Lan or MeLan rings) [6, 7].

Within the bacteria, lanthipeptide operons are organized as biosynthetic gene clusters (cluster I-V), in which the precursor peptide (LanA) is located with the enzymes for modification, transport (LanT), processing (LanP), and regulation (LanR and LanK). In class I and II, genes for immunity against lanthipeptides can be found for (LanI and or LanFEG) [8]. Here LanI is encoding a lipoprotein, which binds the lanthipeptide, and an ABC transporter LanFEG, which expels the lanthipeptide from the membrane, inhibiting pore formation.

The best described lantibiotic is nisin [9], which is naturally produced by several *Lactococcus lactis* strains. It comprises 34 amino acids, which form five lanthionine rings, and has a broad spectrum of activity, inhibiting the growth of Gram-positive and Gram-negative bacteria [10]. Nisin acts as a membrane-targeting peptide and has two main mechanisms of action: **I)** it can bind to the pyrophosphate groups of Lipid II, which is an essential carrier for bacterial cell wall synthesis, thereby sequestering synthesis and halting cell division, and **II)**, nisin/Lipid II complexes embedded in the bacterial membrane can oligomerize leading to the formation of lethal pores [11]. Hence, nisin has both bacteriostatic and bacteriolytic effects, which makes it a highly potent (activity in the low nM range) antibacterial compound [12].

Due to its high potency, high stability, and broad spectrum of activity, nisin has important industrial applications. Currently, it is the only bacteriocin approved by the FDA to

be used as a food preservative [13]. Moreover, intensive research has been performed to bolster its clinical use, especially, against therapy-resistant bacteria such as methicillin-resistant *Staphylococcus aureus* (MRSA) [14].

In their natural environments, bacteria use antibiotic production as a means to eliminate closely related competition from a given niche [15]. It is therefore essential that they possess adequate molecular machinery to protect themselves from the detrimental effects of their own antimicrobial compounds. For this reason, within the nisin biosynthesis operon, there is a set of genes that are responsible for conferring immunity to the producing strain [16]. These genes encode for a membrane-anchored protein (LanI) known as NisI and an ABC transporter (LanFEG) known as NisFEG [17].

NisI is a 27 kDa protein with a membrane anchoring region located at the N-terminus and two extracellular β-barrel domains [18]. Current evidence points toward this protein acting as a nisin binder, preventing its interaction with lipid II [19, 20]. Structural data suggest that the binding of nisin to NisI occurs through a binding cleft located between the two β-barrel domains [18] but the C-terminal domain alone is also capable of interacting with the lantibiotic [19].

NisFEG is an ABC transporter belonging to the LanFEG family [21]. The complex is formed by three protein chains, encoded by the genes *nisF*, *nisE*, and *nisG*. The functional channel is organized as a heterotetrameric structure with stoichiometry 2(F):1(E):1(G). This arrangement places NisFEG within type V of ABC transporters, according to the classification scheme proposed by C. Thomas *et al.* [22]. NisG and NisE constitute the transmembrane region of the transporter, while NisF is intracellularly located and forms a homodimer. The dimer contains the nucleotide binding domains (NBD) that hydrolyze ATP to drive the activity of the transporter. Experimental work showed that NisFEG, as well as other members of the LanFEG family, such as NukFEG, actively remove the lantibiotic from the cellular membrane of *L. lactis* [21, 23]. Recently, the nisin-like biosynthetic gene clusters have been identified in a widely diverse set of organisms, including human pathogenic strains [24], where the presence of, e.g., the *lanfeg* genes is used for the identification of these clusters in the genomic background.

To date, no 3D structure has been experimentally resolved for any member of the LanFEG family. Therefore, the mechanistic details of how the transporter works remain unknown. So far, the sequence-based analysis combined with homology modeling has revealed the presence of a conserved E-loop in LanF proteins. This region is a variation of the conserved Q loop motif observed in other ABC transporters and is essential for conferring immunity against nisin, but not for ATP hydrolysis, implying a role in the conformational rearrangements required for

112 effective antibiotic removal [25]. Previous work established that the C-terminus of nisin plays
113 an important role in the recognition between NisFEG and the lantibiotic, as nisin variants
114 lacking the terminal region were still deadly against cells expressing NisFEG [26]. Similarly,
115 nisin variants varying the crucial hinge region in nisin or a natural variant of nisin produced by
116 another strain are less well recognized by NisFEG indicating a certain degree of substrate
117 specificity [27, 28]. This suggested that NisFEG specifically targets the pore formation mode
118 of action, which is mediated by the C-terminus of nisin. However, the lack of structural
119 information on NisFEG, combined with the large size of nisin, has hindered the development
120 of a hypothesis that can explain the function of the transporter.

121 Here, we constructed a full structural model of the ABC transporter NisFEG in its closed
122 conformation bound to ATP. By using molecular dynamics simulations, we provide first
123 insights into the possible role of the E-loop in the channel's function. Furthermore, by
124 combining co-solvent MD simulations and mutational studies, we were able to identify a
125 putative binding region for nisin.

126

127 **Results**

128 *Architecture of the NisFEG transmembrane domain and full-length model of NisFEG*

129 Models of the transmembrane region of the transporter, involving chains E and G, were
130 generated using two machine learning-based protein structure prediction tools: AlphaFold2 and
131 RoseTTAFold [29]. To have a comparable quality metric between the generated models, the
132 resulting complexes were assessed using TopScore [30] (Supplementary Figure 1). Overall,
133 both AlphaFold2 and RoseTTAFold yield high-quality models containing only small loop
134 regions with low confidence. Subsequent work was carried out using the models generated by
135 RoseTTAFold, as this model showed slightly better scores at the interfacial regions. Then, we
136 searched for remote structurally homologous ABC transporters whose structure-function
137 relationship has been better described, using FoldSeek [31] with NisG as query and the PDB100
138 [31] as target database. Two bacterial proteins were identified that have transporter functions
139 similar to NisFEG: the exporter of virulent peptides PmtCD from *Staphylococcus aureus* [32]
140 (PDB ID 6XJH) and the O-antigen exporter from *Aquifex aeolicus* [33] (PDB ID 7K2T).

141 Comparing the generated NisFEG models with the structures of the homologous
142 transporters reveals that the general architecture of the different transmembrane chains is
143 conserved. In all cases, the five transmembrane helices within a protein chain are arranged in a

144 similar way (Figure 1A). However, the relative orientation of the helices in the oligomeric
145 assembly differs between the two experimentally determined structures. In PDB ID 7K2T, the
146 protein-protein interface is formed by the direct contact of helices αT1 and αT5 of each
147 opposing chain, whereas in PDB ID 6XJH, the contact is mostly mediated by the two αT5
148 helices of each chain (Figure 1B, upper). A cross-section, perpendicular to the helices at the
149 center of the membrane, reveals a significantly smaller surface contact area between the protein
150 chains in PDB ID 6XJH than in PDB ID 7K2T (1193.9 $Å^2$ vs. 1384.7 $Å^2$, respectively, assessed
151 by PDBePISA [34]) (Figure 1B). Furthermore, this difference in helical arrangement leads to
152 the presence of a large cleft located between the chains of PDB ID 6XJH. Both models of the
153 NisEG assembly are structurally more similar to this arrangement. Accordingly, they have a
154 dimerization interface similar to the one observed in PDB ID 6XJH, with most of the interaction
155 being mediated by the αT5 helix. This also leads to the formation of a cleft in the interface
156 region.

157 Considering the overall similar arrangement of the transmembrane domains of the NisEG
158 models and PDB ID 6XJH and that the latter was solved bound to a non-hydrolysable ATP
159 analog, we used PDB ID 6XJH as a template to generate a full model of the entire NisFEG
160 transporter complex in an ATP-bound conformation using RosettaCM [35]. We used this model
161 to investigate the structure-function relationship further. The quality of the resulting complex
162 was evaluated using TopModel, a Ramachandran plot assessment, and the QMean score
163 (Supplementary Figure 2), which are within the normal range for naturally occurring proteins.

164 *Assessing the functional relevance of the conserved E-loop*

165 The NBD contains a catalytically important histidine (H181), which, when mutated, abolishes
166 ATPase hydrolysis, resulting in a transport-deficient variant, which is well known for ABC
167 transporters [26]. On top of this, the LanFEG family possesses a unique structural element
168 known as the E-loop. The name of the loop derives from a conserved Glu residue at the center.
169 So far, this residue is the only amino acid that has been experimentally shown to be essential
170 for the function of the tetramer, but not for ATP hydrolysis [25]. To investigate the structural
171 role of this residue, we performed microsecond-long all-atom molecular dynamics (MD)
172 simulations of the full-length model of NisFEG bound to ATP and embedded in a DMPC
173 membrane bilayer, a composition that has been used in *in vitro* characterizations of other ABC
174 transporters from *L. lactis* [36]. The simulations for the whole complex reach a state of low
175 structural variance after ~200 ns (Supplementary Figure 3).

176 The E-loop is located where the transmembrane chains and the NisF subunits meet (Figure 2A).
177 Here, Glu76 can form electrostatic interactions with Asn72 and Gln75 located in a short
178 intracellular helix of NisG, and Lys129 from the opposing subunit of NisF (Figure 2B).
179 Interestingly, no equivalent interactions between the complementary NisF subunit and NisE
180 were observed. As expected, the structural model of the complex shows that the E-loop residue
181 Glu76 does not interact directly with ATP in the nucleotide-bound conformation
182 (Supplementary Figure 4), consistent with the NisF homolog NukF retaining its catalytic
183 activity when the corresponding residue is mutated [25].

184 To evaluate the persistence of the interactions mediated by Glu76, we measured the distance
185 between its carboxylate side-chain group and the functional groups of the side-chains of the
186 corresponding interacting amino acids. The time series of the interactions reveals a highly
187 dynamic behaviour, where Glu76 is constantly transitioning from low-distance to high-distance
188 configurations to each one of the putative interaction partners (Supplementary Figure 5). A
189 cumulative histogram of the distance of each pair (Figure 2C) reveals that Glu76 spends 93.5%
190 of the simulation times at distances below 10 Å from Gln75, 43.1% at distances lower than 7
191 Å, and 1.5% at distances below 4 Å, with a similar but slightly lower trend observed for Asn72,
192 suggesting that Glu76 plays a role in mediating the interactions between the sub-units of the
193 complex. To add further evidence to the importance of Glu76, we calculated a dynamical cross-
194 correlation matrix (DCCM) for the C_α carbons of the whole complex. A DCCM allows us to
195 identify which elements within a protein are moving in a synchronous (correlated) way
196 throughout an MD trajectory [37]. A cross-correlation index equal to 1 indicates that the
197 movement of the atom pair is correlated, an index of -1 indicates that the movement is anti-
198 correlated, and an index of 0 indicates that the movements of the atom pair are independent
199 from one another. Therefore, interactions that are strong enough will cause correlated
200 movements of the interacting elements. Figure 3 shows the DCC indexes for all residues within
201 a radius of 15 Å of Glu76 of each subunit, mapped onto each chain of the complex. The
202 strongest correlations for the first NisF subunit are observed in the short intracellular helix of
203 NisG, where residues Asn72 and Gln75 are located.

204 On the other hand, the correlation index between Glu76 of the second NisF chain and the
205 equivalent helical segment in NisE is much lower, and stronger correlations occur only
206 intramolecularly, which suggests that there is no strong interaction between the E-loop in the
207 second NBD and NisE.

208 To further support the functional relevance of the intermolecular interactions formed by
209 Glu76 and the NisF subunits, we analysed the degree of evolutionary conservation of the
210 involved residues. As the E-loop has already been established as a conserved element within
211 LanFEG transporters, we focused on the interaction partners located at the small helical
212 segments of NisG. To do this, we employed GEMME[38], a program that predicts mutational
213 outcomes by modeling the evolutionary history of sequences through the construction of
214 phylogenetic trees. We hypothesize that if the interactions between NisG and NisF are relevant,
215 the GEMME score should reflect this in terms of a high probability of functional disruption
216 upon mutation due to the conservation of the residue position. For comparison, we also
217 calculated the GEMME scores for the residues in the equivalent loop of NisE (Figure 4).
218 Residues Asn72 and Gln75 display low GEMME scores observed in NisG (Figure 4A),
219 indicating that these sites are likely to disrupt protein function if mutated. On the other hand, in
220 NisE, the residues predicted with the lowest GEMME scores are Ala72 and Phe75. Both
221 residues point away from $NisF_E$, and Phe75 acts as a hydrophobic contact point to the
222 membrane.

223 Finally, we experimentally tested the impact of mutating one of the interacting partners
224 of the E-loop (Asn72, in NisG) to an alanine residue. As a control, we also mutated the most
225 prominent and conserved polar residue of the equivalent segment of NisE, Gln76, for which
226 GEMME also predicted a high likelihood of functional alteration upon mutation. The complex
227 variants were expressed in *L. lactis*, and the survivability against nisin was measured. Replacing
228 Gln76 with Alanine in NisE does not affect the functioning of NisFEG (Table I). However, the
229 mutation $NisG_{N72A}$ led to a reduction of the base activity of about 25%.

230 Together, these results show that the E-loop is an asymmetric interface element that directly
231 interacts with NisG but does not display the same interaction pattern with NisE.

232 <u>Co-solvent MD simulations and mutational analysis to identify putative regions in</u>
233 <u>NisFEG interacting with nisin</u>

234 So far, there is no evidence on where and how NisFEG binds to nisin. To generate a
235 hypothesis of where the binding interface might be located, we employed cosolvent MD
236 simulations [39]. In this technique, small molecule probes that mimic the main chemical
237 moieties of a ligand are placed in the simulation box and allowed to freely diffuse and interact
238 with the protein surface. Since ligand binding sites provide a chemical environment favorable
239 for non-covalent interactions, the small probes will accumulate in them. This technique has
240 been proven effective to identify previously uncharacterized orthosteric and allosteric sites [39,

241 40]. Since nisin is a highly hydrophobic molecule and rich in peptide bonds, we utilized
242 benzene, *N*-methylacetamide, acetone, and methanol as probes (Figure 5A). We performed five
243 independent simulation replicas of 500 ns length per probe in the same explicit membrane used
244 above and then analyzed in which regions of the complex the accumulation of the different
245 probes overlapped. The convergence of the simulation results was assessed by monitoring the
246 radial distribution function of each probe and by inspecting the change of normalized density
247 pattern over the simulation course (Supplementary Figure 6).

248 Overall, NisFEG accumulates more probes at its transmembrane region than at its
249 intracellular domains, as only minor densities of acetone were observed at NisF (Figure 5B). In
250 the transmembrane region, only one side of the complex displayed a high accumulation of
251 benzene. This site is located between helices αT4 and αT5 of NisE and sits within the interfacial
252 cleft shown in Figure 1B. Nearby, methanol and acetone probes also accumulated. Adjacent to
253 this site, *N*-methylacetamide accumulates at the interface of the subunits near the extracellular
254 side. These results strongly suggest the presence of a binding interface located mainly on NisE,
255 at one of the clefts near the interface between the chains.

256 To further support the hypothesis that this region is a binding interface for nisin, we
257 performed an Alanine scanning mutagenesis experiment and tested whether the function of the
258 transporter was affected. Interestingly, NisE has a high amount of exposed aromatic side-chains
259 in the aforementioned site. Since these residues would provide the highest contact surface area
260 for a putative interaction with nisin, we decided to substitute Trp141, Trp152, Trp179, Tyr184,
261 and Tyr186 for Alanine. As a control, we also mutated the only two Tryptophan residues
262 observed in the opposite cleft of NisG: Trp173 and Trp197. These residues are located in a
263 similar region near helix αT4 of NisG. Therefore, in comparison to the residues on NisE, this
264 should allow us to disentangle whether the functional impacts are chain-specific or if they result
265 from an overall distortion of the protein fold. The variants of the channel were expressed in
266 *L. lactis,* which were then incubated in a medium containing nisin. The resulting bacterial
267 growth was used as a proxy for the activity of the transporter by normalizing against the growth
268 of the strain with WT NisFEG (Figure 5C and Table II).

269 Out of the five positions mutated on NisE, three reduced the function of the transporter
270 to less than 15% of the basal WT activity, with the most drastic change observed for Trp141,
271 resulting in an activity decrease of ~93%. On the other hand, both mutations on NisG reduced
272 the activity to only ~50% of the basal WT activity. Overall, this experiment showed that
273 mutations in the area surrounding the site identified through co-solvent MD simulations have a

274 larger impact on transporter function than mutations in a similar region of the complementing
275 subunit.

276

277 Discussion

278 In this work, we constructed a full model of the lantibiotic transporter NisFEG from *L.*
279 *lactis* and focused our analysis on two unknown aspects of it: what is the role of the conserved
280 E-loop, and where could the putative binding site of nisin be located.

281 A structure-based search using NisG as the query allowed us to identify a distant
282 homolog that also exports a highly lipophilic membrane-disrupting peptide, the ABC
283 transporter PmtCD; a sequence-based search would not have allowed us to identify the homolog
284 due to a sequence identity of only 15.5%. In both cases, the architecture of the transmembrane
285 region of the complex follows a similar arrangement, which results in a narrow interface with
286 prominent clefts at the sides. Zeytuni *et al.* had highlighted the possibility that these side clefts
287 could act as the binding sites for the target peptide [32]. This is a reasonable hypothesis given
288 that the substrate of PmtCD is a hydrophobic helical peptide that embeds itself within the lipid
289 bilayer. This makes the conventional inward-open cavity commonly observed in other ABC
290 transporters for soluble substrates unnecessary, since the peptide cargo already resides in the
291 membrane. Furthermore, eukaryotic ABC transporters that export large hydrophobic
292 substances, such as the ABCA1 transporter, also display a narrow interface mediated mostly by
293 a single helix and large lateral surface clefts [41]. Moreover, the cryo-EM structure of this
294 distantly homologous transporter revealed lipid-like densities at the lateral clefts. It has also
295 been proposed that other ABC transporters, including ABCB4, can function as phospholipid
296 floppases through interactions mediated by the lateral helices [42]. Overall, the current
297 knowledge on ABC transporters suggests that whenever hydrophobic substrates need to be
298 translocated, they are transported directly from the membrane through interactions with the side
299 of the protein. Thus, it is likely that the whole LanFEG family follows a similar mechanism.

300 One aspect that makes transporters of the LanFEG family different from other members
301 of the type V class of ABC transporters is the presence of two distinct transmembrane chains
302 instead of a homodimeric transmembrane region. NisG and NisE share a low sequence identity
303 of 20% but the heterodimer is required for a functional transporter, suggesting that natural
304 selection has led to the divergence of the two chains. Interestingly, our MD simulations revealed
305 that one of the most conserved elements of the LanFEG family, the E-loop of the NBD, interacts

306 differentially with either transmembrane subunit, even though there are two copies of the loop
307 at equivalent positions within the complex. The E-loop is located near a short intracellular α-
308 helix present in both transmembrane subunits, but only NisG forms direct polar contacts with
309 the central Glu76 of the E-loop, which results in a strong coupling of movements between the
310 two proteins. Given that this glutamic acid is essential for the channel function, the E-loop
311 element likely plays a key role in the propagation of conformational rearrangements triggered
312 by the hydrolysis of ATP towards the transmembrane region that are required for effective nisin
313 removal. However, the precise nature and extent of conformational rearrangements that happen
314 at the transmembrane section remain an open question within the LanFEG family.

315 The lack of structural information, combined with the large size and complexity of nisin,
316 has so far hindered the proposal of a possible binding mode. The comparative structural analysis
317 pointed to the lateral cleft of the transporter being a likely binding region. To check if the clefts
318 have suitable physicochemical properties to support nisin binding, we performed co-solvent
319 MD simulations to see whether probes derived from nisin accumulated in these regions, an
320 approach that has been shown to be successful in identifying ligand binding sites [43]. Our
321 results showed a significantly larger and more varied accumulation of probes within the
322 transmembrane region, at the mentioned clefts, than at the intracellular nucleotide binding
323 domain. The accumulation of probes was asymmetric, where a single cleft, dominated by the
324 surface of NisE, retained most probes. That way, one transmembrane chain (NisG) has stronger
325 interactions with NisF, whereas the other (NisE) has stronger interactions with nisin. This
326 asymmetry of interactions could provide an interesting explanation of why there is such a low
327 sequence identity between NisG and NisE; evolution has optimized each chain to perform a
328 specific part of the nisin removal process. Heteromeric complexes formed by homologous
329 chains with low identity are relatively common. For instance, heterodimeric and
330 heterotretrameric ABC transporters are often found in eukaryotic cells, where subunit
331 heterogeneity has been proposed as a means for regulating and fine-tuning the function of the
332 complex [44, 45]. Because the efficacy of a lantibiotic is inherently constrained by the capacity
333 of the producing cell to withstand the toxicity of its own product, there is a strong purging,
334 selective pressure driving the optimization of the immunity-related proteins. Therefore, fine-
335 tuning each transmembrane subunit to drive a specific part of the process could be a favorable
336 evolutionary adaptation.

337 Previous work has shown that the last six residues of the C-terminus of nisin are essential
338 to trigger the activity of NisFEG [26]. Therefore, it could be possible that only the site on the
339 transporter highlighted by our co-solvent MD simulations is involved in initiating the extrusion

process. However, we cannot rule out that throughout the extrusion process, major conformational rearrangements that promote interactions between nisin and other regions of the complex, including NisG, may occur. Nonetheless, in line with our previous argument, it has been shown that multimeric binding sites evolve at a slower rate, as simultaneous mutations in different genes may be required to impact the evolutionary fitness of the complex [46]. This may add another reason why segregation of functionality and a more restricted binding site within the complex may have been favoured by evolution.

To further add substance to our hypothesis that NisE is the chain driving the interactions with nisin, we mutated the residues near the co-solvent hot-spots to check if the function of the complex was affected and compared this with the results of analogous mutations on NisG. Our current experimental setup does not allow us to completely rule out the possibility that the loss of activity observed in the alanine scanning variants might be related to a destabilization of the protein helices. If this were the case, we would expect that both NisG and NisE are destabilized to a similar degree, given that some of the residues mutated are in almost equivalent positions within the protein structure. Thus, we suggest that the driving force of the activity loss is not a decrease in protein stability but a loss of interactions with the lantibiotic.

Taken together, our results represent the first step in constructing a structural hypothesis of how the LanFEG family of ABC transporters, and more specifically NisFEG, confer immunity to lantibiotic-producing bacterial strains.

Materials and Methods

Modeling of NisFEG

A structural model of the transmembrane region involving the protein chains NisE (NCBI: WP_014570414.1) and NisG (NCBI: WP_017864242.1) was generated with RoseTTAFold [29] using HHblits [47] as a sequence search engine, as well as with AlphaFold2 implemented in the Colabfold webserver [48]. The best model out of the two was selected by the lower average TopScore.

The search for further homologous proteins was performed using the FoldSeek [31] webserver with default parameters and the best resulting NisG and NisE models generated by RoseTTAFold as input. The structure of the PmtCD transporter (PDB ID 6XJH) was used as a template for further modeling of the whole complex.

Template-based modeling was performed using the hybridization method in RosettaCM [35], the structure of PDB ID 6XJH, and the RoseTTAFold model of the transmembrane region as templates. The target (including NisF, NCBI: WP_017864240.1) and the template chains were aligned using the PRALINE webserver [49], with PSIPRED [50] and HHMTOP transmembrane region predictions [51] as structural feature guides. The 3-mer and 9-mer were picked based on secondary structure predictions from the PSIPRED and RaptorX [52] web servers. Parameters and centroid information for the Mg-ATP ligands were generated using the molfile_to_params.py script from Rosetta tools. The transmembrane region spans were identified using OPM [53]. 1000 models were generated using the hybridization protocol in two stages, plus a third relaxation stage with membrane weights. The ten best scoring models were selected and subjected to a FastRelax relaxation with membrane penalty scores [54], generating five structures per initial structure. The model with the best Rosetta energy score was used for subsequent work. The quality of the models was assessed using TopScore [30], QMEANBrane [55], and by generating a Ramachandran plot (https://github.com/Joseph-Ellaway/Ramachandran_Plotter).

Conventional and cosolvent all-atom molecular dynamics simulations.

The protonation state of the protein was assigned using Propka in Schrödinger [56]. The model was embedded in a DMPC membrane bilayer using PACKMOL-Memgen [57] and TIP3P as the water model. The orientation of the protein within the membrane was previously determined using the OPM-PPM webserver [53]. Topology and coordinates files were generated using tleap [58]. The forcefield ff19SB [59] was used for the protein and lipid17 [60] for the membrane. The parameters for Mg-ATP were taken from the Bryce database [61, 62]. Counterions were added to maintain the electroneutrality of the system. All simulation work was performed using Amber22 [63]. The initial minimization of the system was performed by adapting the protocol from Roe & Brooks [64], consisting of a total of twelve individual stages. First, 5000 steps of steepest descent minimization followed by 15000 steps of conjugated gradient minimization with positional restraints with a force constant of 5 kcal mol^{-1} $Å^{-2}$ placed on all solute atoms was carried out. Then, the system was heated from 0 to 300 K in an NVT ensemble in a window of 20 ps with a time step of 1 fs, using a Langevin thermostat [65] with a gamma coefficient of 1 ps^{-1}, keeping the same restraints in place. Then three successive minimizations of 1000 steps of steepest descent were performed, reducing the restraints on the solute atoms to 2, 0.1, and 0 kcal mol^{-1} $Å^{-2}$. Afterward, an NPT run of 300 ps with a time step of 1 fs was performed, using an anisotropic Monte-Carlo barostat with a pressure relaxation time of 2 ps and a constant temperature of 300 K with a restraint of 1 kcal mol^{-1} $Å^{-2}$ over solute atoms, followed by another

405 identical run but with a lower restraint of 0.8 kcal mol^{-1} $Å^{-2}$. Five subsequent NPT runs of the
406 same length and time steps were performed, placing the restraints only on the protein atoms and
407 decreasing the force constant by 0.2 kcal mol^{-1} $Å^{-2}$ each run until reaching 0 kcal mol^{-1} $Å^{-2}$.
408 Production runs were performed for 1 μs with a time step of 2 fs using the GPU-accelerated
409 implementation of pmemd [66]. The first 10 ns of production were run with a positional restraint
410 of 0.1 kcal mol^{-1} $Å^{-2}$ on protein atoms and a width of the non-bonded skin of 5 Å and discarded
411 from further analysis. Five independent replicas were carried out saving the coordinates of the
412 system every 100 ps. All simulations were performed using the SHAKE algorithm [67] to
413 constrain the length of bonds to hydrogens and a non-bonded cut-off of 10 Å.

414 Distances between residues throughout the simulations were calculated using the *distance*
415 command in cpptraj [68]. The distances were calculated between the centre of mass of the
416 carboxylic oxygens of Glu76 and the centre of mass of nitrogen and oxygen of the amide group
417 from either Asn72 or Gln75, or the sidechain nitrogen from Lys129. A per-residue cross-
418 correlation matrix was calculated using the *matrix* command in cpptraj. To suppress spurious
419 correlations, we used only the 80% of the total frames with the lowest RMSD with respect to
420 the starting configuration,

421 For cosolvent MD simulations, the systems were prepared using acetone, benzene, methanol,
422 or *N*-methylacetamide as a probe. The placement of the probe molecules was performed using
423 PACKMOL-Memgen in a ratio of 1 molecule of co-solvent per 99 molecules of water, using
424 the same membrane and solvent as described previously. The parameters for each co-solvent
425 are included within PACKMOL-Memgen. Five independently packed systems were generated
426 for each probe to randomize the initial position of the probes. The same minimization,
427 thermalization, and pressurization protocol as previously described was used. Five independent
428 production replicas per random packing were carried out, utilizing the same conditions as
429 previously described, but with a production run length of 500 ns. The density distributions for
430 each probe were calculated by first aligning the backbone atoms of the protein using the *rms*
431 command in cpptraj and wrapping the solvent and cosolvent molecules with the *autoimage*
432 function. Densities were calculated using the *grid* command in cpptraj, with a 340 Å length in
433 each direction and a grid spacing of 0.5 Å and frame number normalization. The hot spots
434 within the protein surface were selected using AQUA-DUCT [69], using the *pond_run*
435 command. To assess convergence, the grid calculation was repeated at different total simulation
436 times (100, 200, 300, 400, and 500 ns) to assess the invariance of the density distribution. Also,
437 the radial distribution function for each probe was calculated against the Cα atoms of the protein

438 in a window of 100 Å, using the *radial* command on cpptraj, ignoring intramolecular
439 interactions.

440 **Site-directed mutagenesis, protein expression, and measurement of NisFEG activity**

441 NisE, NisG, and NisF (or the inactive variant $NisF_{H181A}$, to generate a sensitive control) were
442 cloned into a pILSV shuttle vector as previously described elsewhere [26]. Site-directed
443 mutagenesis was performed by PCR using Phusion DNA polymerase, the template NisFEG-
444 pILSV vector, and a mutagenic primer pair (Table 3). The mutated plasmids were transformed
445 into *L. lactis* NZ9000 by electroporation at 1 kV, 25 µF, 5.0 msec.

446 Nisin was purified and quantified as described elsewhere [70]. The transformed *L. lactis* strains
447 harbouring either the WT or a variant were grown overnight in GM17 media supplemented with
448 10 µg / mL chloramphenicol in the presence of 1 ng / mL of nisin for inducing expression. The
449 next day, the cells were diluted to an OD_{600} of 0.1 in fresh GM17 media and incubated for 30
450 minutes at 30 °C. Then, 150 µL of bacterial sample were loaded into a 96-well plate alongside
451 50 µL of nisin solution. The samples were incubated for 5-7 hours at 30°C, and the OD_{600} was
452 measured. The activities of NisFEG, control strain, and mutants were calculated as described
453 in previous work [71].

454

ASSOCIATED CONTENT

Supporting Information

Supporting Information is available free of charge at: [XXX: Add link to paper.]

Supplementary figures and supplementary references (PDF).

AUTHOR INFORMATION

Corresponding Authors

H.G.:

Address: Universitätsstr. 1, 40225 Düsseldorf, Germany.

Phone: (+49) 211 81 13662

E-mail: gohlke@uni-duesseldorf.de

ORCID

Holger Gohlke: 0000-0001-8613-1447

Author Contributions

Conceptualization, PAC, HG; methodology, PAC (modeling and simulations), JG (biochemistry); writing - original draft preparation, PAC, HG; writing - review and editing, JG, SHJS; data analysis and interpretation, PAC, JG, SHJS, HG; supervision and project administration, SHJS, HG; funding acquisition, SHJS, HG. All authors have read and agreed to the published version of the manuscript.

Funding Sources

This research was funded by grants from the Deutsche Forschungsgemeinschaft [DFG, German Research Foundation; 270650915/GRK 2158 (to HG, SHJS)]. The Center for Structural Studies is funded by the Deutsche Forschungsgemeinschaft [DFG; 417919780 (to SHJS)].

Notes

The authors declare no competing financial interest.

Acknowledgements

We are grateful for computational support and infrastructure provided by the "Zentrum für Informations- und Medientechnologie" (ZIM) at the Heinrich Heine University Düsseldorf and the computing time provided by the John von Neumann Institute for Computing (NIC) to HG on the supercomputer JUWELS at Jülich Supercomputing Centre (JSC) (user ID: VSK33).

DATA AND SOFTWARE AVAILABILITY STATEMENT

The software used for generating the models is in the public domain. The Schrödinger software is available here: https://www.schrodinger.com/ . The AMBER package of molecular simulation codes is available here: https://ambermd.org/ . Source data, input files, and processing scripts are available at researchdata.hhu.de under https://researchdata.hhu.de/handle/entry/196 .

References

1. Goto, Y., et al., *Discovery of unique lanthionine synthetases reveals new mechanistic and evolutionary insights.* PLoS Biol, 2010. **8**(3): p. e1000339.
2. Tracanna, V., et al., *Mining prokaryotes for antimicrobial compounds: from diversity to function.* FEMS Microbiol Rev, 2017. **41**(3): p. 417-429.
3. Li, B., et al., *Catalytic promiscuity in the biosynthesis of cyclic peptide secondary metabolites in planktonic marine cyanobacteria.* Proc Natl Acad Sci U S A, 2010. **107**(23): p. 10430-5.
4. Gross, E. and J.L. Morell, *The presence of dehydroalanine in the antibiotic nisin and its relationship to activity.* J Am Chem Soc, 1967. **89**(11): p. 2791-2.
5. Gross, E. and J.L. Morell, *The number and nature of alpha,beta-unsaturated amino acids in nisin.* FEBS Lett, 1968. **2**(1): p. 61-64.
6. Li, B., et al., *Structure and Mechanism of the Lantibiotic Cyclase Involved in Nisin Biosynthesis.* Science, 2006. **311**(5766): p. 1464-1467.
7. Negash, A.W. and B.A. Tsehai, *Current Applications of Bacteriocin.* Int J Microbiol, 2020. **2020**: p. 4374891.
8. Smits, S.H.J., L. Schmitt, and K. Beis, *Self-immunity to antibacterial peptides by ABC transporters.* FEBS Lett., 2020. **594**(23): p. 3920-3942.
9. Willey, J.M. and W.A.v.d. Donk, *Lantibiotics: Peptides of Diverse Structure and Function.* Annu. Rev. Microbiol., 2007. **61**(1): p. 477-501.
10. Cheigh, C.-I. and Y.-R. Pyun, *Nisin Biosynthesis and its Properties.* Biotechnol. Lett., 2005. **27**(21): p. 1641-1648.
11. Medeiros-Silva, J., et al., *High-resolution NMR studies of antibiotics in cellular membranes.* Nat. Commun., 2018. **9**(1): p. 3963.
12. Wiedemann, I., et al., *Specific Binding of Nisin to the Peptidoglycan Precursor Lipid II Combines Pore Formation and Inhibition of Cell Wall Biosynthesis for Potent Antibiotic Activity* *. J. Biol. Chem., 2001. **276**(3): p. 1772-1779.
13. Gharsallaoui, A., et al., *Nisin as a Food Preservative: Part 1: Physicochemical Properties, Antimicrobial Activity, and Main Uses.* Crit. Rev. Food Sci. Nutr., 2016. **56**(8): p. 1262-1274.
14. Cotter, P.D., C. Hill, and R.P. Ross, *Bacterial lantibiotics: strategies to improve therapeutic potential.* Curr Protein Pept Sci, 2005. **6**(1): p. 61-75.
15. Stubbendieck, R.M. and P.D. Straight, *Multifaceted Interfaces of Bacterial Competition.* J Bacteriol, 2016. **198**(16): p. 2145-55.
16. Siegers, K. and K.D. Entian, *Genes involved in immunity to the lantibiotic nisin produced by Lactococcus lactis 6F3.* Applied and Environmental Microbiology, 1995. **61**(3): p. 1082-1089.
17. Stein, T., et al., *Function of Lactococcus lactis Nisin Immunity Genes nisI and nisFEG after Coordinated Expression in the Surrogate Host Bacillus subtilis.* J. Biol. Chem., 2003. **278**(1): p. 89-94.
18. Jeong, J.H. and S.C. Ha, *Crystal Structure of NisI in a Lipid-Free Form, the Nisin Immunity Protein, from Lactococcus lactis.* Antimicrob Agents Chemother, 2018. **62**(3).
19. Hacker, C., et al., *The Solution Structure of the Lantibiotic Immunity Protein NisI and Its Interactions with Nisin.* J Biol Chem, 2015. **290**(48): p. 28869-86.
20. Takala, T.M., et al., *Lipid-free NisI: interaction with nisin and contribution to nisin immunity via secretion.* FEMS Microbiol. Lett., 2004. **237**(1): p. 171-177.
21. Alkhatib, Z., et al., *Lantibiotics: How do producers become self-protected?* J. Biotechnol., 2012. **159**(3): p. 145-154.
22. Thomas, C., et al., *Structural and functional diversity calls for a new classification of ABC transporters.* FEBS Lett., 2020. **594**(23): p. 3767-3775.
23. Okuda, K., et al., *Cooperative transport between NukFEG and NukH in immunity against the lantibiotic nukacin ISK-1 produced by Staphylococcus warneri ISK-1.* J Bacteriol, 2008. **190**(1): p. 356-62.
24. Hourigan, D., et al., *Nisin-like biosynthetic gene clusters are widely distributed across microbiomes.* mBio, 2025: p. e0154525.
25. Okuda, K., et al., *Functional significance of the E loop, a novel motif conserved in the lantibiotic immunity ATP-binding cassette transport systems.* J Bacteriol, 2010. **192**(11): p. 2801-8.

26. AlKhatib, Z., et al., *The C-terminus of nisin is important for the ABC transporter NisFEG to confer immunity in Lactococcus lactis.* Microbiologyopen, 2014. **3**(5): p. 752-763.
27. Reiners, J., et al., *Insights in the Antimicrobial Potential of the Natural Nisin Variant Nisin H.* Front Microbiol, 2020. **11**: p. 573614.
28. Zaschke-Kriesche, J., et al., *Influence of nisin hinge-region variants on lantibiotic immunity and resistance proteins.* Bioorg Med Chem, 2019. **27**(17): p. 3947-3953.
29. Baek, M., et al., *Accurate prediction of protein structures and interactions using a three-track neural network.* Science, 2021. **373**(6557): p. 871-876.
30. Mulnaes, D. and H. Gohlke, *TopScore: Using Deep Neural Networks and Large Diverse Data Sets for Accurate Protein Model Quality Assessment.* J. Chem. Theory Comput., 2018. **14**(11): p. 6117-6126.
31. van Kempen, M., et al., *Fast and accurate protein structure search with Foldseek.* Nat Biotechnol, 2024. **42**(2): p. 243-246.
32. Zeytuni, N., et al., *Structural insight into the Staphylococcus aureus ATP-driven exporter of virulent peptide toxins.* Sci Adv, 2020. **6**(40).
33. Caffalette, C.A. and J. Zimmer, *Cryo-EM structure of the full-length WzmWzt ABC transporter required for lipid-linked O antigen transport.* Proc Natl Acad Sci U S A, 2021. **118**(1).
34. Krissinel, E. and K. Henrick, *Inference of macromolecular assemblies from crystalline state.* J Mol Biol, 2007. **372**(3): p. 774-97.
35. Song, Y., et al., *High-resolution comparative modeling with RosettaCM.* Structure, 2013. **21**(10): p. 1735-42.
36. Siarheyeva, A., J.J. Lopez, and C. Glaubitz, *Localization of Multidrug Transporter Substrates within Model Membranes.* Biochemistry, 2006. **45**(19): p. 6203-6211.
37. Yu, H. and P.A. Dalby, *A beginner's guide to molecular dynamics simulations and the identification of cross-correlation networks for enzyme engineering.* Methods Enzymol, 2020. **643**: p. 15-49.
38. Laine, E., Y. Karami, and A. Carbone, *GEMME: A Simple and Fast Global Epistatic Model Predicting Mutational Effects.* Molecular Biology and Evolution, 2019. **36**(11): p. 2604-2619.
39. DasGupta, D., et al., *Identifying Potential Ligand Binding Sites on Glycogen Synthase Kinase 3 Using Atomistic Cosolvent Simulations.* ACS Appl Bio Mater, 2024. **7**(2): p. 588-595.
40. Ghanakota, P. and H.A. Carlson, *Moving Beyond Active-Site Detection: MixMD Applied to Allosteric Systems.* J Phys Chem B, 2016. **120**(33): p. 8685-95.
41. Qian, H., et al., *Structure of the Human Lipid Exporter ABCA1.* Cell, 2017. **169**(7): p. 1228-1239.e10.
42. Prescher, M., et al., *Evidence for a credit-card-swipe mechanism in the human PC floppase ABCB4.* Structure, 2021. **29**(10): p. 1144-1155.e5.
43. Arcon, J.P., et al., *Molecular Dynamics in Mixed Solvents Reveals Protein-Ligand Interactions, Improves Docking, and Allows Accurate Binding Free Energy Predictions.* J Chem Inf Model, 2017. **57**(4): p. 846-863.
44. Sudha, G., N. Naveenkumar, and N. Srinivasan, *Evolutionary and structural analyses of heterodimeric proteins composed of subunits with same fold.* Proteins, 2015. **83**(10): p. 1766-86.
45. Hillebrand, M., et al., *Live cell FRET microscopy: homo- and heterodimerization of two human peroxisomal ABC transporters, the adrenoleukodystrophy protein (ALDP, ABCD1) and PMP70 (ABCD3).* J Biol Chem, 2007. **282**(37): p. 26997-27005.
46. Abrusan, G. and J.A. Marsh, *Ligand Binding Site Structure Influences the Evolution of Protein Complex Function and Topology.* Cell Rep, 2018. **22**(12): p. 3265-3276.
47. Remmert, M., et al., *HHblits: lightning-fast iterative protein sequence searching by HMM-HMM alignment.* Nat Methods, 2011. **9**(2): p. 173-5.
48. Mirdita, M., et al., *ColabFold: making protein folding accessible to all.* Nat Methods, 2022. **19**(6): p. 679-682.
49. Bawono, P. and J. Heringa, *PRALINE: a versatile multiple sequence alignment toolkit.* Methods Mol Biol, 2014. **1079**: p. 245-62.
50. McGuffin, L.J., K. Bryson, and D.T. Jones, *The PSIPRED protein structure prediction server.* Bioinformatics, 2000. **16**(4): p. 404-5.

51. Tusnady, G.E. and I. Simon, *The HMMTOP transmembrane topology prediction server.* Bioinformatics, 2001. **17**(9): p. 849-50.
52. Kallberg, M., et al., *RaptorX server: a resource for template-based protein structure modeling.* Methods Mol Biol, 2014. **1137**: p. 17-27.
53. Lomize, M.A., et al., *OPM database and PPM web server: resources for positioning of proteins in membranes.* Nucleic Acids Res, 2012. **40**(Database issue): p. D370-6.
54. Fleishman, S.J., et al., *RosettaScripts: a scripting language interface to the Rosetta macromolecular modeling suite.* PLoS One, 2011. **6**(6): p. e20161.
55. Studer, G., M. Biasini, and T. Schwede, *Assessing the local structural quality of transmembrane protein models using statistical potentials (QMEANBrane).* Bioinformatics, 2014. **30**(17): p. i505-i511.
56. Olsson, M.H., et al., *PROPKA3: Consistent Treatment of Internal and Surface Residues in Empirical pKa Predictions.* J Chem Theory Comput, 2011. **7**(2): p. 525-37.
57. Schott-Verdugo, S. and H. Gohlke, *PACKMOL-Memgen: A Simple-To-Use, Generalized Workflow for Membrane-Protein-Lipid-Bilayer System Building.* J Chem Inf Model, 2019. **59**(6): p. 2522-2528.
58. Case, D.A., et al., *AmberTools.* J Chem Inf Model, 2023. **63**(20): p. 6183-6191.
59. Tian, C., et al., *ff19SB: Amino-Acid-Specific Protein Backbone Parameters Trained against Quantum Mechanics Energy Surfaces in Solution.* J Chem Theory Comput, 2020. **16**(1): p. 528-552.
60. Dickson, C.J., R.C. Walker, and I.R. Gould, *Lipid21: Complex Lipid Membrane Simulations with AMBER.* J Chem Theory Comput, 2022. **18**(3): p. 1726-1736.
61. Meagher, K.L., L.T. Redman, and H.A. Carlson, *Development of polyphosphate parameters for use with the AMBER force field.* J Comput Chem, 2003. **24**(9): p. 1016-25.
62. Allner, O., L. Nilsson, and A. Villa, *Magnesium Ion-Water Coordination and Exchange in Biomolecular Simulations.* J Chem Theory Comput, 2012. **8**(4): p. 1493-502.
63. Salomon-Ferrer, R., et al., *Routine Microsecond Molecular Dynamics Simulations with AMBER on GPUs. 2. Explicit Solvent Particle Mesh Ewald.* J Chem Theory Comput, 2013. **9**(9): p. 3878-88.
64. Roe, D.R. and B.R. Brooks, *A protocol for preparing explicitly solvated systems for stable molecular dynamics simulations.* J Chem Phys, 2020. **153**(5): p. 054123.
65. Quigley, D. and M.I. Probert, *Langevin dynamics in constant pressure extended systems.* J Chem Phys, 2004. **120**(24): p. 11432-41.
66. Harris, J.A., et al., *GPU-Accelerated All-Atom Particle-Mesh Ewald Continuous Constant pH Molecular Dynamics in Amber.* J Chem Theory Comput, 2022. **18**(12): p. 7510-7527.
67. Kräutler, V., W.F. van Gunsteren, and P.H. Hünenberger, *A fast SHAKE algorithm to solve distance constraint equations for small molecules in molecular dynamics simulations.* J. Comput. Chem., 2001. **22**(5): p. 501-508.
68. Roe, D.R. and T.E. Cheatham, 3rd, *PTRAJ and CPPTRAJ: Software for Processing and Analysis of Molecular Dynamics Trajectory Data.* J Chem Theory Comput, 2013. **9**(7): p. 3084-95.
69. Magdziarz, T., et al., *AQUA-DUCT: a ligands tracking tool.* Bioinformatics, 2017. **33**(13): p. 2045-2046.
70. Abts, A., et al., *Easy and Rapid Purification of Highly Active Nisin.* Int. J. Pept, 2011. **2011**(1): p. 175145.
71. Gottstein, J., Zaschke-Kriesche, J., Unsleber, S. et al. *New insights into the resistance mechanism for the BceAB-type transporter SaNsrFP.* Sci. Rep., 2022. **12**: p. 4232.

650 # Tables

651

652 **Table 1**. Site-directed mutagenesis at the intracellular NisG helix impairs NisFEG function.

	NisFEG control	$NisF_{H118A}$	$NisG_{N72A}$	$NisE_{Q76A}$
IC_{50} (nM)	118	12	93	118
F. o. R[1]	10	1	8	10
Activity (%)	100	0	76	100

653 [1.] Factor of resistance.

654

655 **Table 2**. Activity of alanine scanning variants.

NisFEG variant	Activity (%)
NisFEG WT	100 [1]
$NisF_{H118A}$	23.5
$NisG_{W173A}$	48.5
$NisG_{W197}$	50.0
$NisE_{W141A}$	7.3
$NisE_{W152A}$	37.7
$NisE_{W179A}$	11.7
$NisE_{Y184A}$	64.4
$NisE_{Y186A}$	10.2

656 [1] The activity of the WT was set to 100%.

657

658 **Table 3.** Mutagenic primers used in the present study.

Primer	Sequence (5'-3')
NisF_N72A-for	GAGTCTGGCCGCACGTTTCCAAG
NisF_N72A_rev	TCCTGTTCAAAGATTAGAATAG
NisF_Q76A_for	TGGAAATTTTGCAAATGTGAAATGGAAAAAG
NisF_Q76A_rev	GCTTGCTCCTCTGATTTTATATC
NisF-H181A-for	GACAATCTTGATTTCTAGTGCTCAGTTGCACGAAATAAGTAAAG
NisF-H181A-rev	CTTTACTTATTTCGTGCAACTGAGCACTAGAAATCAAGATTGTC
NisE-W141A-for	TACTAGCAGCTTCTGCTAATTTACCCTTTATATAC
NisE-W141A-rev	GTATATAAAGGGTAAATTAGCAGAAGCTGCTAGTA
NisE_W152A_for	CTTTATATACTTGATTTTCAAGGCTATTAATACTTACGTATTG
NisE_W152A_rev	CAATACGTAAGTATTAATAGCCTTGAAAATCAAGTATATAAAG
NisE-W179A-for	GCACAAACTCCAGTAGCTTTCTTGCTACC
NisE-W179A-rev	GGTAGCAAGAAAGCTACTGGAGTTTGTGC
NisE_Y184A-for	CAGTATGGTTCTTGCTACCAGCTACTTATCACTATAAAG
NisE_Y184A-rev	CTTTATAGTGATAAGTAGCTGGTAGCAAGAACCATACTG
NisE_Y186A -rev	CTGTAACTTTATAGTGAGCAGTGTATGGTAGCAAGAACC
NisE_Y186A-for	GGTTCTTGCTACCATACACTGCTCACTATAAAGTTACAG
NisG_W173A_for	GTTTTATTAGCAGCTTATGCTTGTCCTATTGCTTTAC
NisG_W173A_rev	GTAAAGCAATAGGACAAGCATAAGCTGCTAATAAAAC
NisG_W197A_for	GATAGCTGCCGTAGGGGCTATTGTTTTATCCAC
NisG_W197A_rev	GTGGATAAAACAATAGCCCCTACGGCAGCTATC

659

660 **Figures**

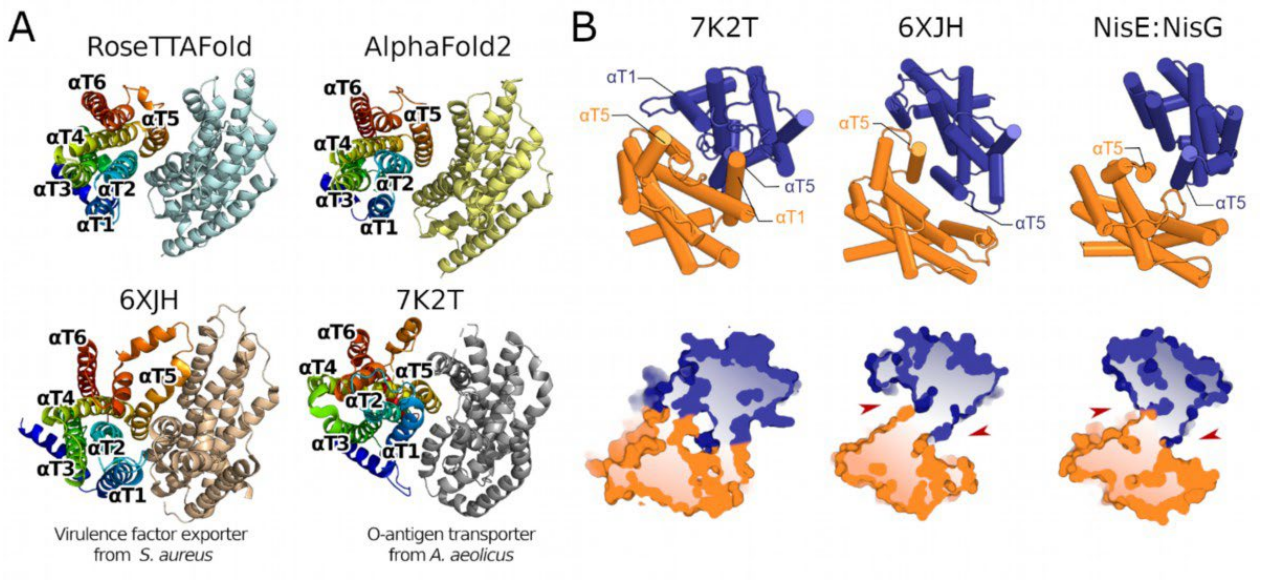

Figure 1. Architecture of the transmembrane region of NisFEG. A) Structural models for NisE:NisG generated with RoseTTAFold and AlphaFold2 (upper panel, left and right, respectively) compared with experimentally determined structures of the virulence factor exporter PmtCD (lower left panel; PDB ID 6XJH) and the O-antigen transporter Wzm/Wzt (lower right panel; PDB ID 7K2T). The left chain is colored from the N-terminus (blue) to the C-terminus (red). B) The upper row shows a cartoon representation of 7K2T, 6XJH, and NisE:NisG (RoseTTAFold model) highlighting the interfacial helixes. The lower panels depict a perpendicular cross-section of each complex. Pronounced clefts are highlighted with red arrowheads. For the NisE:NisG complex, the first chain is shown in orange and the latter in blue.

661

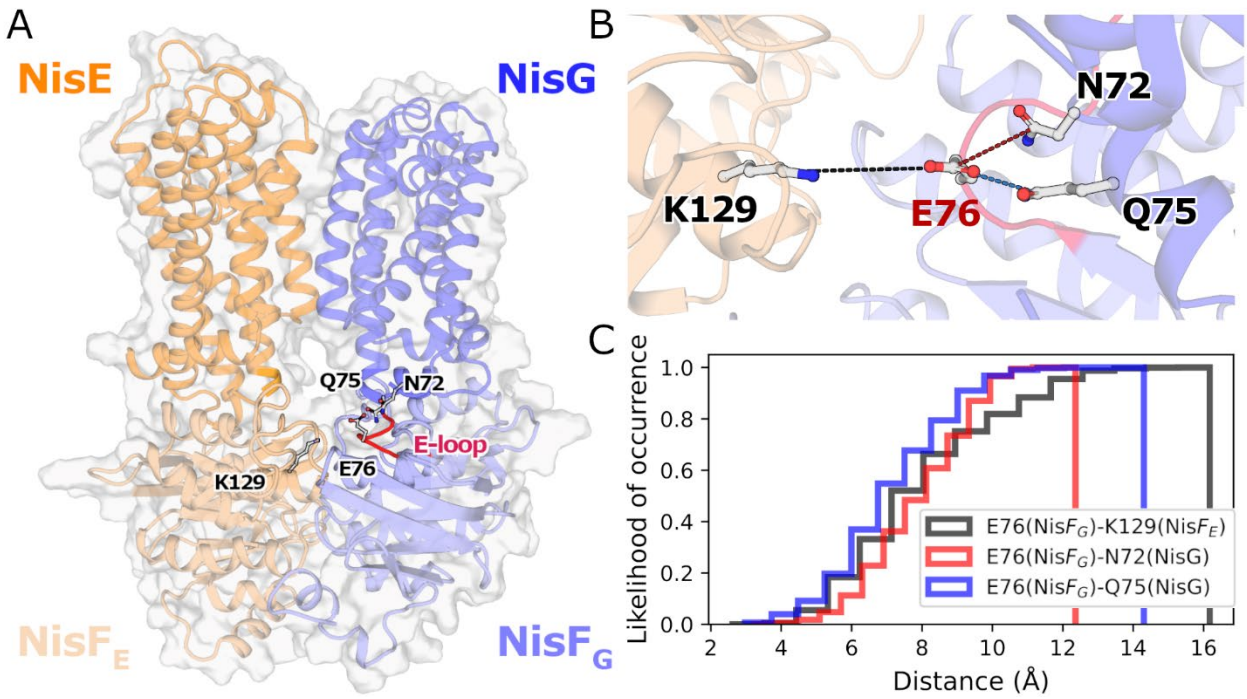

Figure 2. The E-loop mediates interactions with NisG. A) Global view of the NisFEG complex model, with the E-loop of a NisF chain highlighted in pink. Residues participating in interactions are labeled. B) Close-up of the electrostatic interactions formed by Glu76 with Lys129 of the other NisF subunit (black dashed line), and Asn72 and Gln75 of NisG (red and blue dashed lines, respectively). C) Cumulative histogram of the distances between the residues shown in panel B observed in MD simulations.

662

663

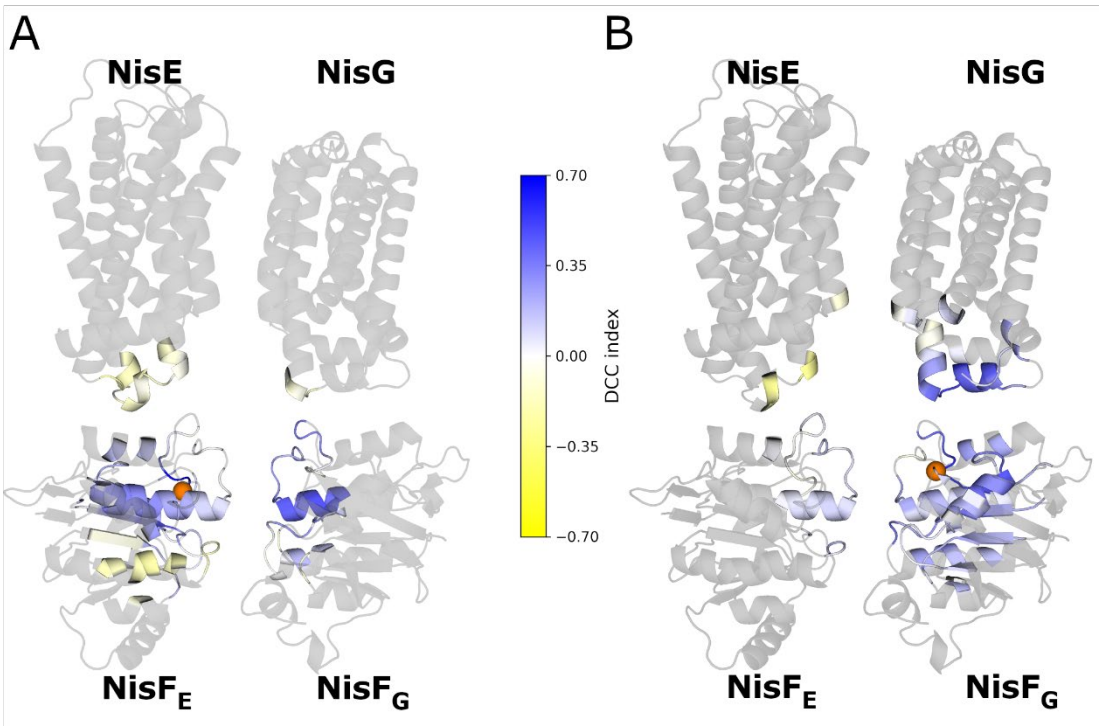

Figure 3. Movements of the E-loop are correlated to those in NisG but not in NisE. A) View of each individual chain of NisFEG. Residues within a radius of 15 Å of the central E-loop residue Glu76 (C_α atom highlighted as orange sphere) are colored according to their dynamic cross correlation (DCC) index. The dark blue regions are the ones moving in parallel to Glu76. B) Same as in A, but highlighting the residues surrounding Glu76 in the E-loop of the second NisF sub-unit. The same color scale applies for both panels.

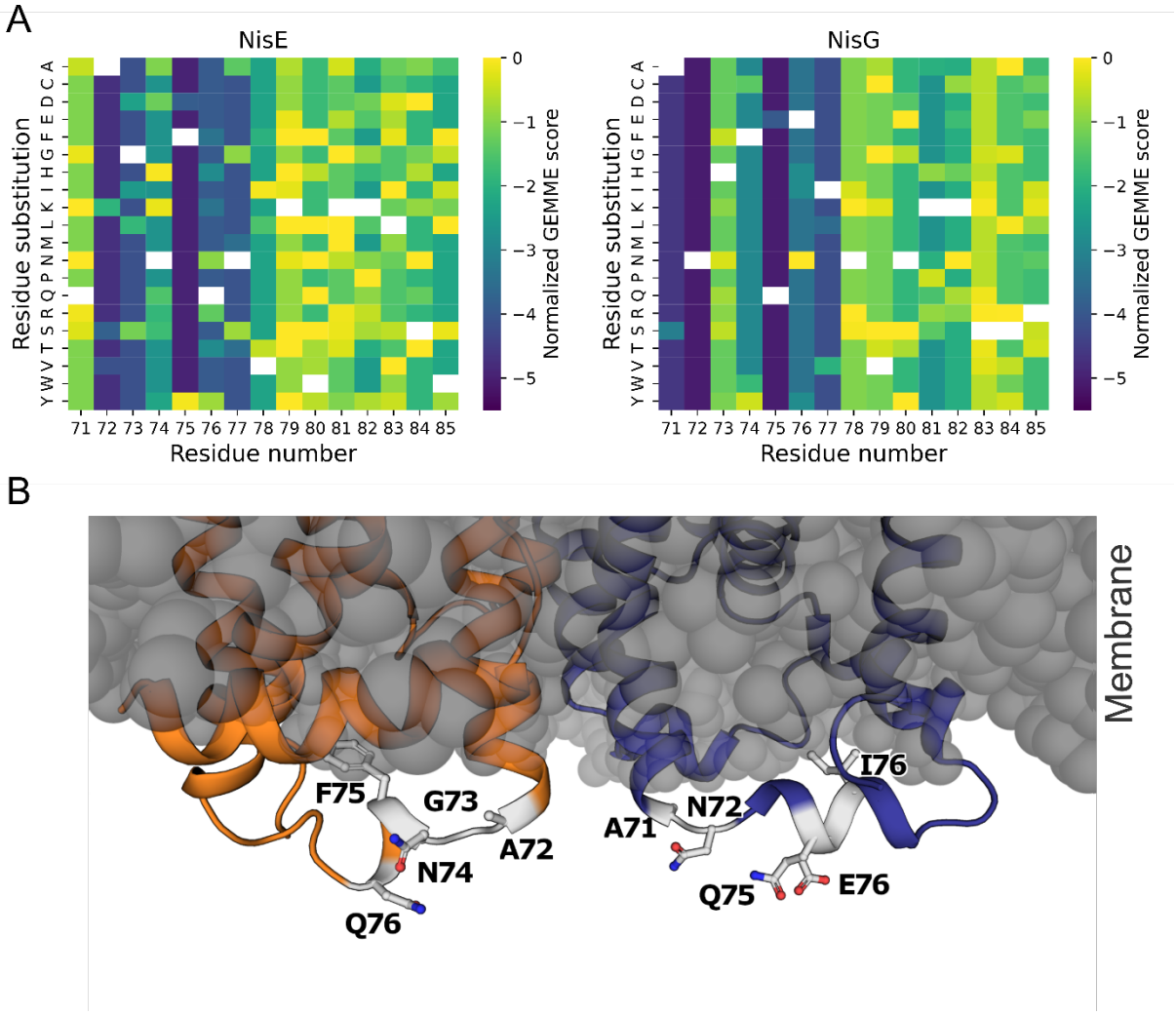

Figure 4. Solvent-exposed residues on the intracellular helix of NisG are more conserved and their loss could lead to functional disruption. A) GEMME score for residues belonging to the NisE intracellular helix. Lower scores indicate a higher degree of conservation and, therefore, a higher likelihood of a residue being functionally relevant. B) Structural view of the residues with strong predicted functional relevance (white sticks) for NisE (orange cartoon) and NisG (blue cartoon).

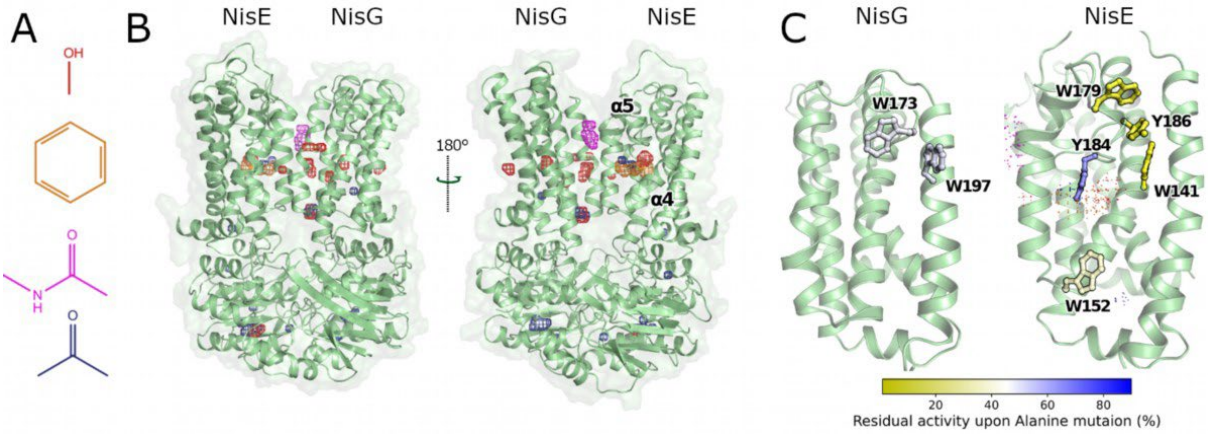

Figure 5. Co-solvent MD simulations and mutational analysis suggest a putative nisin binding site. A) Co-solvent probes used for MD simulations. B) Density distribution of co-solvents across the complex; the helixes near the highest accumulations on NisE are labeled. The densities for each probe follow the same color scheme as in A (red: methanol, yellow: benzene, magenta: *N*-methylacetamide, blue: acetone). C) Residual activities upon alanine mutation. The WT residues replaced for alanine in each variant are shown as sticks. The color scale shows the percentage of activity observed in the Ala-containing variant relative to the WT.

673